

# Microbiome subcommunity learning with logistic-tree normal latent Dirichlet allocation

Patrick LeBlanc

Department of Statistical Sciences, Duke University

and

Li Ma\*

Department of Statistical Sciences, Duke University

November 12, 2021

## Abstract

Mixed-membership (MM) models such as Latent Dirichlet Allocation (LDA) have been applied to microbiome compositional data to identify latent subcommunities of microbial species. These subcommunities are informative for understanding the biological interplay of microbes and for predicting health outcomes. However, microbiome compositions typically display substantial cross-sample heterogeneities in subcommunity compositions—that is, the variability in the proportions of microbes in shared subcommunities across samples—which is not accounted for in prior analyses. To address this limitation, we incorporate the logistic-tree normal (LTN) model into LDA to form a new MM model. This model allows cross-sample variation in the composition of each subcommunity around some “centroid” composition that defines the subcommunity. Incorporation of auxiliary Pólya-Gamma variables enables a computationally efficient collapsed blocked Gibbs sampler to carry out Bayesian inference under this model. We compare the LDA and the new model and show that in the presence of large cross-sample heterogeneity, LDA can produce inference which is sensitive to the specification of the number of subcommunities. As such, the popular strategy of overspecifying the number of subcommunities and hoping that some meaningful subcommunities will emerge alongside artificial ones can lead to misleading conclusions. In contrast, by accounting for such heterogeneity, our new model restores the robustness of the inference in the specification of the number of subcommunities and allows meaningful subcommunities to be identified.

*Keywords:* Mixed-membership models, latent variable models, compositional data, Bayesian inference

---

\*Email: li.ma@duke.edu

# 1 Introduction

The human gut microbiome is the genetic content of all bacteria, archaea, viruses, and eukaryotic microbes residing in the human gut and is commonly used to profile the composition of the gut microbiota: the set of all such microbes. Advances in next-generation sequencing techniques have substantially reduced the cost of this approach and made it widely accessible. One highly cost-effective microbiome profiling strategy is based on targeting a single marker gene, namely the 16S ribosomal RNA (rRNA) gene, through amplicon-based sequencing [Li, 2015]. A more expensive, but more precise, approach is whole-genome shotgun metagenomic sequencing [Beghini et al., 2021]. Traditionally, sequencing reads have been clustered into Operational Taxonomic Units (OTUs), which serve as the basic unit of microbial taxa. Recently, amplicon sequencing variants (ASVs) have come into wider use as they can achieve more precise characterization of microbial species and resolve the sample-specificity issue of the OTU [Callahan et al., 2017]. Our work is applicable to either method of characterizing microbial taxa; in the following we shall generically refer to the basic unit as ASVs.

Gut microbiome studies often involve highly heterogeneous samples due to the multitude of factors that can influence an individual’s gut microbiota. A useful analytical method for analyzing microbiome compositions is thus to classify microbiome samples into clusters characterized by a particular compositional signature. In the context of gut microbiome, these clusters are called “enterotypes” [Costea et al., 2018] and have been found to be associated with various health outcomes [Del Chierico et al., 2014]. A number of microbiome clustering methods have been introduced in recent years. One of the simplest and most popular methods is the Dirichlet-multinomial mixture (DMM) model [Holmes et al., 2012, Nigam

et al., 2000], which uses a hierarchical structure to allow within-cluster sample-to-sample variability in subcommunity compositions. However, the DMM is too restrictive to realistically characterize the within-cluster, cross-sample variance present in microbiome data [Tang et al., 2018, Wang and Zhao, 2017] as it uses a single scalar parameter to characterize the entire covariance structure across the microbial taxa. More general methods have recently been introduced to alleviate, though not eliminate, this limitation through the use of Dirichlet-tree models [Mao et al., 2020, Wang and Zhao, 2017].

Such clustering analysis, however, makes the implicit assumption that each microbiome sample must belong to a *single* signature “community” characterized by the cluster centroid. This assumption is often unrealistic and overly restrictive for complex environments such as the gut microbiome [Holmes et al., 2012, Mao et al., 2020]. Recent developments embrace the more relaxed biological hypothesis that the ASVs characterizing a microbiota sample hail from a combination of multiple microbial “clusters”, or more precisely “subcommunities”.

Mixed-membership (MM) models are a generalization of clustering models which allow samples to have fractional membership in clusters. MM models provide a generative modeling framework for data involving subcommunity structure by allowing each microbiome sample to be composed of multiple microbial subcommunities. Sankaran and Holmes [2019] applied the most well-known MM model, the latent Dirichlet allocation (LDA) model, to microbiome profiling, while Shafiei et al. [2015] and Deek and Li [2019] proposed variations of LDA accounting for environmental factors and inflated zero-counts, respectively.

The key motivation for our paper is the observation that existing MM models such as LDA—originally developed for other contexts such as topic modeling and population genetics—do not incorporate key features of microbiome compositions. Most notably, they

assume that a microbial subcommunity’s composition must remain *exactly the same* across all samples. This is unrealistic in the vast majority of microbiome studies collected from diverse environments such as the gut where samples often display high levels of heterogeneity. It is interesting to note that such heterogeneity has been well-recognized in clustering models for microbiome data [Holmes et al., 2012, Mao et al., 2020], but to date has been largely ignored in existing application of MM models. Additionally, in applications of MM models such as in topic modelling, it is a common practice to overspecify the number of “topics”—the analogue to subcommunities—in the hope that some meaningful “topics” will emerge amongst others. We will demonstrate that this practice can lead to misleading inferences in the microbiome context if cross-sample heterogeneity is not properly accounted for.

We introduce a generalization to the LDA model that aims to appropriately incorporate “random effects”, i.e., cross-sample heterogeneity in microbiomal subcommunity compositions due to unmeasured sources, thereby leading to more accurate identification of subcommunities in MM models. Our approach takes advantage of the availability of a natural tree structure relating the microbial taxa—the phylogenetic tree—which allows us to decompose the compositional vector into a collection of binomial observations, one for each of the tree nodes. This transform serves two purposes. First, it allows us to model the heterogeneity by modeling the vector of log-odds transforms of the binomial probabilities at each node as multivariate Gaussian. By modeling the subcommunity compositions as realizations from this logistic-tree normal (LTN) [Wang et al., 2021] distribution, we are able to impose appropriate constraints on the underlying covariance structure to ensure the identifiability of the subcommunities. A second purpose of the tree-based transform is computational. By utilizing the so-called Pólya-Gamma (PG) data augmentation technique [Polson et al., 2013],

Bayesian inference under the resulting MM model can be readily accomplished through fully conjugate collapsed blocked Gibbs sampling. We term our new model logistic-tree normal latent Dirichlet allocation (LTN-LDA).

In the following, we will briefly review the LDA and LTN models before introducing the LTN-LDA model. We will augment the LTN-LDA model using a class of auxiliary Pólya-Gamma variables [Polson et al., 2013] and present a collapsed blocked Gibbs sampler for carrying out Bayesian inference. We will demonstrate in simulations that in the presence of cross-sample heterogeneity the inference produced by LTN-LDA is robust with respect to overspecifying the number of subcommunities while inference under LDA can be highly sensitive. We will then apply LTN-LDA to the dataset of Dethlefsen and Relman [2011], which has been used for demonstrating MM models in the microbiome settings [Sankaran and Holmes, 2019], and compare our results to prior analyses.

## 2 Methods

### 2.1 Latent Dirichlet allocation

Let there be  $D$  samples consisting of counts of  $V$  unique ASVs indexed by  $1, 2, \dots, V$ . For sample  $d$ , let  $\mathbf{x}_d = (x_{d,1}, \dots, x_{d,V})$  be the vector of ASV counts such that  $x_{d,v}$  is the total count for ASV  $v$  in sample  $d$ . Let  $N_d = \sum_{v=1}^V x_{d,v}$  be the sum of counts in sample  $d$ , which is determined by the sequencing depth.

Subcommunities are defined to be collections of ASVs that co-occur in samples at given relative proportions. The composition of a subcommunity is the relative proportions of the ASVs within that subcommunity. An ASV can occur in multiple subcommunities at various abundances and the key assumption underlying an MM model, in contrast to a clustering

model, is that different instances (i.e., the sequencing read counts) of the same ASV in a sample can arise from the participation of that ASV in multiple microbial subcommunities. Key parameters of interest in MM models are subcommunity abundance, i.e., the proportions of the various subcommunities in each sample, and subcommunity composition, i.e., the proportions of the ASVs in each subcommunity.

To describe LDA, it is convenient to introduce multinomial-Bernoulli indicators for each read count and its associated subcommunity identity. For  $d = 1, 2, \dots, D$ , let  $\mathbf{w}_d$  be a vector  $\mathbf{w}_d = (w_{d,1}, \dots, w_{d,N_d})$  where  $w_{d,n} \in \{1, 2, \dots, V\}$  is multinomial-Bernoulli indicator of the ASV associated with the  $n$ th read count in the sample. We refer to the elements  $w_{d,n}$  in this vector as “tokens” to draw analogy with other areas of MM model application. In topic modelling, each token is a word in a document; here, each token corresponds to a read count associated with an ASV in a sample. We also note that  $x_{d,v} = \sum_{n=1}^{N_d} \mathbf{1}_{\{w_{d,n}=v\}}$ .

Let  $\boldsymbol{\phi}_d = (\phi_d^1, \phi_d^2, \dots, \phi_d^K)' \in \Delta^{K-1}$ , where we use  $\Delta^S$  to denote the  $S$ -dimensional simplex, be the subcommunity abundance vector. That is,  $\phi_d^k$  represents the relative abundance of subcommunity  $k$  in sample  $d$ , and so  $\boldsymbol{\phi}_d$  specifies the multinomial-Bernoulli distribution of each token over the  $K$  underlying subcommunities in sample  $d$ . Let  $z_{d,n}$  represent the subcommunity from which the  $n^{th}$  token in sample  $d$  arises from and let  $\mathbf{z}_d$  be the vector all such assignments for sample  $d$ . Also, let  $\boldsymbol{\beta}_k = (\beta_k^1, \beta_k^2, \dots, \beta_k^V)' \in \Delta^{V-1}$  be the subcommunity composition for subcommunity  $k$ . That is,  $\boldsymbol{\beta}_k$  gives the relative proportions of the  $V$

unique ASVs in subcommunity  $k$ . The LDA model [Blei et al., 2003] is then

$$\begin{aligned} w_{d,n} | z_{d,n}, \beta_{z_{d,n}} &\stackrel{\text{ind}}{\sim} \text{Mult}(1, \beta_{z_{d,n}}) \\ z_{d,n} | \phi_d &\stackrel{\text{ind}}{\sim} \text{Mult}(1, \phi_d) \\ \phi_d | \alpha &\stackrel{\text{iid}}{\sim} \text{Dir}(\alpha) \\ \beta_k | \gamma &\stackrel{\text{iid}}{\sim} \text{Dir}(\gamma) \end{aligned}$$

for  $d = 1, \dots, D$  and  $n = 1, \dots, N_d$  while  $\alpha$  and  $\gamma$  are hyperparameters. The graphical model is presented in Figure 1a.

Though LDA can be applied in the microbiome context [Sankaran and Holmes, 2019], it does not account for cross-sample heterogeneity in subcommunity composition. In particular, it assumes that the  $\beta_k$  are the *exact same* across all samples. This assumption is inconsistent with the empirical behavior of the microbiome setting where large cross-sample heterogeneities exist [Holmes et al., 2012]. This has two important consequences: LDA interprets cross-sample heterogeneity as the presence of additional subcommunities and thus tends to overestimate the “true” number of subcommunities, especially when the modelled number of subcommunities,  $K$ , is overspecified.

## 2.2 Incorporating cross-sample heterogeneity

We shall enrich the LDA framework to allow cross-sample heterogeneity in the subcommunity compositions. There are several widely used hierarchical models for microbiome compositions in the literature such as the Dirichlet-Multinomial (DM) model [Holmes et al., 2012, Nigam et al., 2000] and Aitchinson’s log-ratio based normal (LN) models [Aitchison, 1982], all of which could be embedded into the LDA for this purpose. However, the DM is highly restrictive in its ability to characterize the underlying cross-sample variability as the

Dirichlet distribution has only a single scalar variance parameter, while the LN models are computationally challenging due to lack of conjugacy to the multinomial sampling model. To resolve these difficulties, we adopt the recently introduced logistic-tree normal (LTN) model [Wang et al., 2021] to obtain both modeling flexibility and computational efficiency. In particular, we will show that the LTN model can be readily embedded into the LDA model to accommodate cross-sample heterogeneity and that posterior inference can be accomplished through simple collapsed blocked Gibbs sampling using a data-augmentation technique called the Pólya-Gamma augmentation. Moreover, we note that, since the adoption of the LTN model requires specifying a dyadic partition tree on the ASVs, the phylogenetic tree relating the taxa is the natural tree structure to use. In the following, we briefly introduce the phylogenetic tree and the LTN model constructed based on the phylogenetic tree, before embedding the LTN model into LDA to form our new MM model.

### 2.2.1 The phylogenetic tree

Let  $\mathcal{T}$  denote a phylogenetic tree encapsulating the evolutionary relationships among the observed ASVs. The leaf nodes in the tree correspond to the observed ASVs in the data set. Each interior node is the inferred common ancestral taxon for the ASVs lying in the corresponding descendant subtree at the node. Each node (or taxon)  $A$  in the phylogenetic tree  $\mathcal{T}$  can be represented by the collection of its descendant ASVs. In particular, each leaf node  $A$  contains a single ASV, whereas each internal node  $A$  contains multiple ASVs. In the following, we let  $\mathcal{L}$  be the set of leaf nodes of  $\mathcal{T}$ , and  $\mathcal{I}$  the internal nodes. Throughout this work, we shall assume that the phylogenetic tree is rooted and binary, in the sense that each interior node  $A$  has exactly two child nodes (i.e., direct descendants). For an example of this notation, see the supporting information section S1.



For each node  $A \in \mathcal{I}$  we let  $A_l$  and  $A_r$  be the left and right children of  $A$ , respectively. For each node  $A \in \mathcal{T}$ , we use  $y(A)$  to denote the total sequencing read counts associated with all ASVs or leaves descended from  $A$ . When there are multiple subcommunities and samples, we extend this notation to  $y_{d,k}(A)$  which is the total sequencing read counts associated with all ASVs or leaves descended from  $A$  in subcommunity  $k$  and sample  $d$ .

### 2.2.2 The LTN model

The LTN model is based on a factorization of the multinomial distribution of ASVs on the leaves of  $\mathcal{T}$  for sample  $d$  and subcommunity  $k$ ,  $\beta_{d,k} = (\beta_{d,k}^1, \beta_{d,k}^2, \dots, \beta_{d,k}^V)' \in \Delta^{V-1}$ , into a set of binomial distributions on the internal nodes  $\mathcal{I}$ . For each internal node  $A \in \mathcal{I}$ , for each sample  $d$ , and for each subcommunity  $k$ , we define

$$\theta_{d,k}(A) = \frac{\sum_{v \in A_l} \beta_{d,k}^v}{\sum_{v \in A} \beta_{d,k}^v},$$

which expresses the probability that a token descended from  $A$  is also descended from  $A_l$  under  $\beta_{d,k}$ . The binomial likelihood at each node is thus

$$y_{d,k}(A_l) \mid y_{d,k}(A), \theta_{d,k}(A) \sim \text{Bin}(y_{d,k}(A) \mid y_{d,k}(A), \theta_{d,k}(A)).$$

Let  $\theta_{d,k}$  be a vector containing the values of  $\theta_{d,k}(A)$  with respect to an ordering on the  $p = |\mathcal{I}|$  internal nodes of  $\mathcal{T}$  and note that  $\theta_{d,k}$  is in one-to-one correspondence with  $\beta_{d,k}$ .

Let  $\psi_{d,k}(A) = \log \frac{\theta_{d,k}(A)}{1 - \theta_{d,k}(A)}$  be the log-odds transform of  $\theta_{d,k}(A)$  and let  $\psi_{d,k}$  be the vector of  $\psi_{d,k}(A)$  with respect to the same ordering on the  $p$  internal nodes of  $\mathcal{T}$ . Then for each  $d$

$$\psi_{d,k} \mid \mu_k, \Sigma_k \stackrel{\text{ind}}{\sim} \text{MVN}(\mu_k, \Sigma_k),$$

for some mean vector  $\mu_k$  and covariance matrix  $\Sigma_k$  associated with subcommunity  $k$ . We

place conjugate priors on  $\boldsymbol{\mu}_k$  and  $\Sigma_k$ , giving rise to a hierarchical LTN model:

$$\begin{aligned}
y_{d,k}(A_l) \mid y_{d,k}(A), \psi_{d,k}(A) &\stackrel{\text{ind}}{\sim} \text{Bin}(y_{d,k}(A), \theta_{d,k}(A)) \\
\boldsymbol{\psi}_{d,k} \mid \boldsymbol{\mu}_k, \Sigma_k &\stackrel{\text{ind}}{\sim} \text{MVN}(\boldsymbol{\mu}_k, \Sigma_k) \\
\boldsymbol{\mu}_k \mid \boldsymbol{\mu}_0, \Lambda_0 &\stackrel{\text{iid}}{\sim} \text{MVN}(\boldsymbol{\mu}_0, \Lambda_0) \\
\Sigma_k \mid F &\stackrel{\text{iid}}{\sim} F,
\end{aligned}$$

for  $d = 1, \dots, D, k = 1, \dots, K$  and  $A \in \mathcal{I}$ , where  $\boldsymbol{\mu}_0$  and  $\Lambda_0$  are hyperparameters and  $F$  is a prior distribution on  $\Sigma$ , which we will specify later.

## 2.3 LTN-LDA

We incorporate the LTN model into LDA to allow cross-sample heterogeneity in subcommunity compositions. The resulting model is termed logistic-tree normal latent Dirichlet allocation (LTN-LDA). Let  $y_{d,k}(A)$  represent the count of all sequencing reads descended from node  $A$  in sample  $d$  assigned to subcommunity  $k$ . Let  $\psi_{d,k}(A) \in \mathbb{R}$  represent the log-odds at node  $A$  and  $\boldsymbol{\psi}_{d,k}$  be the vector of  $\psi_{d,k}(A)$  for each sample  $d$  and subcommunity  $k$ . Let  $\boldsymbol{\mu}_k$  be the vector of average log-odds in subcommunity  $k$ , and let  $\Sigma_k$  be the associated covariance matrix. If there are  $N_d$  ASVs in the  $d^{\text{th}}$  sample then the generative model is

$$\begin{aligned}
y_{d,k}(A_l) \mid y_{d,k}(A), \psi_{d,k}(A) &\stackrel{\text{ind}}{\sim} \text{Bin}(y_{d,k}(A), \theta_{d,k}(A)) \\
z_{d,n} \mid \boldsymbol{\phi}_d &\stackrel{\text{ind}}{\sim} \text{Mult}(1, \boldsymbol{\phi}_d) \\
\boldsymbol{\phi}_d \mid \boldsymbol{\alpha} &\stackrel{\text{iid}}{\sim} \text{Dir}(\boldsymbol{\alpha}) \\
\boldsymbol{\psi}_{d,k} \mid \boldsymbol{\mu}_k, \Sigma_k &\stackrel{\text{ind}}{\sim} \text{MVN}(\boldsymbol{\mu}_k, \Sigma_k), \\
\boldsymbol{\mu}_k \mid \boldsymbol{\mu}_0, \Lambda_0 &\stackrel{\text{iid}}{\sim} \text{MVN}(\boldsymbol{\mu}_0, \Lambda_0) \\
\Sigma_k \mid F &\stackrel{\text{iid}}{\sim} F
\end{aligned}$$

for  $d = 1, \dots, D$ ,  $k = 1, \dots, K$ ,  $n = 1, \dots, N_d$ , and  $A \in \mathcal{I}$ . Note that, for this paper, we set  $\boldsymbol{\mu}_0 = 0$  and assume that  $\boldsymbol{\alpha} = (\alpha, \alpha, \dots, \alpha)$ . We present a graphical model representation for LTN-LDA in Figure 1b. The key distinction between LTN-LDA and LDA is that LTN-LDA uses an LTN to model the varying compositions of each sub community across samples. In particular, the composition in sample  $d$  of subcommunity  $k$  is determined by  $\boldsymbol{\psi}_{d,k}$  and is explicitly allowed to vary across samples.

Without additional assumptions or constraints on the high-dimensional covariance matrices for each subcommunity,  $\Sigma_k$ , the model is generally too flexible, and can even become unidentifiable at sample sizes typical for microbiome studies. Additional structural constraints that serves the purpose of regularization on the covariance structure are thus necessary. We adopt the additional structural constraint that  $\Sigma_k$  is a diagonal covariance matrix. While the assumption may appear overly strong, we note that the dependence among the tree-based log-odds ratios are generally much weaker in comparison to the often very strong and complex dependence structure among the ASV counts themselves. In a sense, the tree-based log-odd transform of the abundance vectors “decorrelates” the data. (For the interested reader, this decorrelation phenomenon is analogous to the so-called “whitening” effects in wavelet analysis, as the dyadic tree transform we incorporate here is the counterpart of Haar-wavelet transform on functions.)

Aside from the diagonal covariance assumption, we also enforce that the amount of variability for each node depends on that node’s distance to the bottom (i.e., leaf) level of the tree. In particular, we assume that taxa close to the bottom of the phylogenetic tree have larger cross-sample variability in the corresponding log-odds ratio than those which are distant. This is consistent with empirical observations, as well as the biological intuition that

taxa which are deep in the tree tend to have comparable functionality. Their relative proportions thus often display elevated levels of variance due to their functional exchangeability.

Specifically, let  $|A|$  measure the distance of  $A$  from the leaf level by denoting the number of leaves descended from node  $A$ . The prior on  $\Sigma_k$  we adopt has the form

$$\begin{aligned}\Sigma_k \mid \boldsymbol{\tau}_k &= \text{diag}(\boldsymbol{\tau}_k) \\ \tau_{i,k} \mid a_1, b &\stackrel{\text{iid}}{\sim} \text{IG}(a_1, b) \quad \text{if } |A_i| \geq C \\ \tau_{i,k} \mid a_2, b &\stackrel{\text{iid}}{\sim} \text{IG}(a_2, b) \quad \text{if } |A_i| < C\end{aligned}$$

for  $i = 1, \dots, p$ ,  $k = 1, \dots, K$ ,  $C \in \mathbb{N}$  (which may be treated as a tuning parameter), and  $\boldsymbol{\tau}_k = (\tau_{1,k}, \dots, \tau_{p,k})$ . This choice of priors ensures conjugate updating, avoids identifiability issues for reasonable hyperparameter values, and allows cross-sample heterogeneity in a biologically justifiable manner. We choose  $a_1$ ,  $a_2$ , and  $b$  such that nodes high in the tree have low expected variance in the posterior, while nodes low in the tree have a high expected variance.

## 2.4 Bayesian inference by collapsed blocked Gibbs sampling

### 2.4.1 Pólya-Gamma latent variables

The LTN-LDA model presented thus far does not induce conjugate full conditionals; to make it so we introduce a class of Pólya-Gamma latent variables [Polson et al., 2013], one for each interior node  $A$ ,  $v_{d,k}(A)$ , which is independent of  $y_{d,k}(A_l)$  conditioned on  $y_{d,k}(A)$  and  $\psi_{d,k}(A)$ :

$$v_{d,k}(A) \mid y_{d,k}(A), \psi_{d,k}(A) \sim \text{PG}(y_{d,k}(A), \psi_{d,k}(A)).$$

The probability density of  $y_{d,k}(A_l)$  conditioned on  $v_{d,k}(A)$  is then proportional to

$$\exp \left( \left( y_{d,k}(A_l) - \frac{y_{d,k}(A)}{2} \right) \psi_{d,k}(A) - \frac{v_{d,k}(A) \psi_{d,k}(A)^2}{2} \right),$$

which is conjugate to the multivariate Gaussian density of  $\psi_{d,k}$ . The graphical model for LTN-LDA with the Pólya-Gamma variables is presented in Figure 1c. For notational purposes let  $\mathbf{v}_{d,k}$  be the vector of  $v_{d,k}(A)$  and let  $\boldsymbol{\kappa}_{d,k}$  be the vector of  $\kappa_{d,k}(A)$ .

#### 2.4.2 Collapsed blocked Gibbs sampler

We integrate the  $\phi_d$  out of the sampling model and proceed with a collapsed Gibbs sampler to improve convergence [Griffiths and Steyvers, 2004]. The full conditionals we will sample from are thus

$$\begin{aligned}
(1) \quad & (\mathbf{v}_{d,k}, \mathbf{z}_d) \mid \psi_{d,k}, \boldsymbol{\mu}_k, \Sigma_k, \Lambda_0, \boldsymbol{\alpha}, a_1, a_2, b \stackrel{\text{ind}}{\sim} p(\mathbf{v}_{d,k}, \mathbf{z}_d \mid \psi_{d,k}, \boldsymbol{\alpha}) \\
(2) \quad & \psi_{d,k} \mid \mathbf{v}_{d,k}, \mathbf{z}_d, \boldsymbol{\mu}_k, \Sigma_k, \Lambda_0, \boldsymbol{\alpha}, a_1, a_2, b \stackrel{\text{ind}}{\sim} p(\psi_{d,k} \mid \mathbf{v}_{d,k}, \mathbf{z}_d, \boldsymbol{\mu}_k, \Sigma_k) \\
(3) \quad & \boldsymbol{\mu}_k \mid \mathbf{v}_{d,k}, \mathbf{z}_d, \psi_{d,k}, \Sigma_k, \Lambda_0, \boldsymbol{\alpha}, a_1, a_2, b \stackrel{\text{ind}}{\sim} p(\boldsymbol{\mu}_k \mid \psi_{d,k}, \Sigma_k, \Lambda_0) \\
(4) \quad & \Sigma_k \mid \mathbf{v}_{d,k}, \mathbf{z}_d, \psi, \boldsymbol{\mu}_k, \Lambda_0, \boldsymbol{\alpha}, a_1, a_2, b \stackrel{\text{ind}}{\sim} p(\Sigma_k \mid \psi, \boldsymbol{\mu}_k, \Lambda_0, a_1, a_2, b),
\end{aligned}$$

The joint full conditional  $(\mathbf{v}_{d,k}, \mathbf{z}_d)$  is

$$\begin{aligned}
& \mathbf{z}_d \mid \psi_{d,k}, \boldsymbol{\alpha} \stackrel{\text{ind}}{\sim} p(\mathbf{z}_d \mid \psi_{d,k}, \boldsymbol{\alpha}) \\
& \mathbf{v}_{d,k} \mid \mathbf{z}_d, \psi_{d,k}, \boldsymbol{\alpha} \stackrel{\text{ind}}{\sim} p(\mathbf{v}_{d,k} \mid \mathbf{z}_d, \psi_{d,k}).
\end{aligned}$$

To sample the vector  $\mathbf{z}_d$  from its full conditional, we sample each subcommunity assignment in order from its multinomial full conditional:

$$p(z_{d,n} = k \mid \mathbf{z}_d^{-n}, \psi_{d,k}, \boldsymbol{\alpha}) \propto (y_{d,k}(\mathcal{R})^{-n} + \alpha) \times \beta_k^{w_{d,n}},$$

where  $\mathbf{z}_d^{-n}$  is the vector of all subcommunity assignments in sample  $d$  except for  $z_{d,n}$  and  $y_{d,k}(\mathcal{R})^{-n}$  is the number of sequencing reads in sample  $d$  descended from the root node  $\mathcal{R}$  assigned to subcommunity  $k$  not counting the  $n^{\text{th}}$  token. To sample from the full conditional for  $\mathbf{v}_{d,k}$ , we draw  $v_{d,k}(A)$  for each  $A \in \mathcal{I}$ :

$$v_{d,k}(A) \mid y_{d,k}(A), \psi_{d,k}(A) \stackrel{\text{ind}}{\sim} \text{PG}(y_{d,k}(A), \psi_{d,k}(A)),$$

the conjugate full conditional of a Pólya-Gamma distribution derived in [Polson et al. \[2013\]](#).

However, existing Pólya-Gamma samplers are slow for the current context and so for large values of  $y_{d,k}(A)$  we use an approximate Pólya-Gamma sampler proposed in [Glynn et al. \[2019\]](#), which uses the normal distribution as an approximation:

$$N\left(\frac{y_{d,k}(A)^2}{2\psi_{d,k}(A)}\tanh\left(\frac{\psi_{d,k}(A)}{2}\right), \frac{y_{d,k}(A)^2}{4\psi_{d,k}(A)^3}\operatorname{sech}^2\left(\frac{\psi_{d,k}(A)}{2}\right)(\sinh(\psi_{d,k}(A)) - \psi_{d,k}(A))\right).$$

The full conditionals for  $\boldsymbol{\mu}_k$  and the  $\tau_{i,k}$  follow by conjugate updating:

$$\begin{aligned}\boldsymbol{\mu}_k \mid \boldsymbol{\psi}_{d,k}, \Sigma_k, \Lambda_0 &\stackrel{\text{ind}}{\sim} \text{MVN}\left((\Lambda_0^{-1} + D\Sigma_k^{-1})^{-1}\Sigma_k^{-1}\sum_{d=1}^D\boldsymbol{\psi}_{d,k}, (\Lambda_0^{-1} + D\Sigma_k^{-1})^{-1}\right) \\ \tau_{i,k} \mid \boldsymbol{\psi}, \boldsymbol{\mu}_k, a_1, a_2, b &\stackrel{\text{ind}}{\sim} \text{IG}\left(a_1 + \frac{D}{2}, \frac{2b + \sum_{d=1}^D(\psi_{d,k}(A_i) - \mu_k(A_i)^2)}{2}\right) \quad \text{if } |A_i| \geq C \\ \tau_{i,k} \mid \boldsymbol{\psi}, \boldsymbol{\mu}_k, a_1, a_2, b &\stackrel{\text{ind}}{\sim} \text{IG}\left(a_2 + \frac{D}{2}, \frac{2b + \sum_{d=1}^D(\psi_{d,k}(A_i) - \mu_k(A_i)^2)}{2}\right) \quad \text{if } |A_i| < C.\end{aligned}$$

Further, the full conditional for  $\boldsymbol{\psi}_{d,k}$  is also multivariate normal,

$$\boldsymbol{\psi}_{d,k} \mid \mathbf{z}_d, \mathbf{v}_{d,k}, \mu_k, \Sigma_k \stackrel{\text{ind}}{\sim} \text{MVN}\left((\Sigma_k^{-1} + \operatorname{diag}(\mathbf{v}_{d,k}))^{-1}(\Sigma_k^{-1}\boldsymbol{\mu}_k + \boldsymbol{\kappa}_{d,k}), (\Sigma_k^{-1} + \operatorname{diag}(\mathbf{v}_{d,k}))^{-1}\right).$$

## 3 Numerical experiments

### 3.1 Robustness in choosing the number of subcommunities

The true number of subcommunities  $K$  in a given dataset is typically unknown, and so a common strategy in application of MM models in contexts such as topic modeling is to overspecify  $K$  and hope that a subset of identified subcommunities will correspond to contextually meaningful ones. However, for data with large cross-sample heterogeneity such as microbiome data, intuition suggests that a model that assumes zero heterogeneity will confuse sample-specific variation around a subcommunity mean with the presence of additional subcommunities, resulting in inference sensitive to the choice of  $K$ .

To verify this intuition, we first generate data from a known LTN-LDA model which induces cross-sample heterogeneity. In particular, we simulate  $D = 50$  samples,  $N_d = 10,000$  ASVs per sample, and set  $\alpha = 1$ ,  $\mu = 0$ ,  $\Lambda = I$ ,  $a_1 = 10^4$ , and  $a_2 = b = 10$ . We set the true number of subcommunities to be  $K = 4$  and the cutoff point to be  $C = 10$ . The underlying phylogenetic tree used is presented in Figure 2: there are 49 leaves and 48 internal nodes, and each color indicates a region where the majority—approximately 77.5 percent—of the total prevalence of a subcommunity composition is located.

We now contrast LDA and LTN-LDA by running collapsed blocked Gibbs samplers on the data generated above with  $K \in \{4, 5, 7, 10\}$ . We start by setting the modelled value of  $C$  in the LTN-LDA sampler equal to truth. (In the next subsection, we will vary the specified  $C$  and examine the effect.) In the left part of Figure 3, we plot the posterior means of the subcommunity abundances  $\phi_d$  for both LDA and LTN-LDA. Note that we can estimate the value of  $\phi_d$  from the  $\mathbf{z}_d$  with

$$\hat{\phi}_d = \frac{1}{\sum_{k=1}^K y_{d,k}(\mathcal{R}) + K\alpha} \left( y_{d,1}(\mathcal{R}) + \alpha, \quad \dots, \quad y_{d,K}(\mathcal{R}) + \alpha \right)'.$$

As there are a small number of topics, we manually correct for label switching by matching the subcommunities according to the ASV compositions.

With  $K$  set to the true value, LDA performs comparably to LTN-LDA in terms of estimating the true values of  $\phi_d$ . However, as we increase  $K$  beyond the true value, the inference provided by LDA worsens. While it still recovers the abundances for subcommunities 1 and 2, it does a worse job at recovering subcommunities 3 and 4. Moreover, LDA detects the presence of additional subcommunities which do not exist in the true generative model. LTN-LDA, in contrast, is remarkably stable when the  $K$  is overspecified: no matter the modelled value

of  $K$ , it detects the four true subcommunities with approximately the same abundances. Additional subcommunities have very little estimated abundance.

For  $K = 10$ , we plotted the ASV-subcommunity distributions on the right part of Figure 3. Distributions for the  $\beta_{d,k}$  are in blue and the  $\beta_k$  are in red for LTN-LDA; the LDA  $\beta_k$  distributions are in black. LTN-LDA finds some moderate levels of cross-sample heterogeneity in subcommunity 2, and a high levels in samples 3 and 4.

These two figures imply that LDA is able to recover the subcommunity abundances only for those subcommunities with low levels of cross-sample heterogeneity. LDA fails to recover the subcommunity abundances for those subcommunities with high levels of cross-sample heterogeneity; it instead mistakes cross-sample heterogeneity as additional subcommunities. In effect, LDA splits true heterogeneous subcommunities into many smaller subcommunities with no heterogeneity and ASVs which ought to belong in the same subcommunity are separated. LTN-LDA, on the other hand, provides stable and accurate inference as the modelled value of  $K$  increases. Thus, if we were to adopt an approach of overestimating the number subcommunities in our model with the hope of recovering meaningful subcommunities in the presence of cross-sample heterogeneity, we will be misled if we ignore such heterogeneity as in LDA. The risk is much lower when we appropriately account for the heterogeneity.

### 3.2 Predictive scoring as a device for choosing tuning parameters

While incorporating cross-sample heterogeneity enhances the robustness of LTN-LDA to overspecifying the number of subcommunities, it is still useful to have a generally applicable strategy for setting the tuning parameters for LTN-LDA:  $K$  and  $C$ . One option is to use out-of-sample predictive performance to identify suitable choices of the tuning parameters.



A popular performance measure for MM models—originally designed for LDA in the topic modeling context—is perplexity [Wallach et al., 2009]: a transform of out-of-sample predictive likelihood such that lower perplexity scores indicate better out-of-sample performance. Details are left to the supporting information, section S2.

We thus examine the simple strategy of computing the average out-of-sample perplexity score for different choices of  $(K, C)$  and examine whether that can lead to a practical way of choosing these parameters. We will also examine whether this strategy could be adopted for models without cross-sample heterogeneity, namely LDA, to eliminate, or at least alleviate, their limitations. We follow the procedure proposed in Section 5.1 of Wallach et al. [2009] for computing the perplexity for LDA, and generalize that strategy to computing the perplexity score for LTN-LDA.

We generate 200 simulated datasets. In each, there are  $D = 50$  samples,  $N_d = 10,000$  ASVs per sample, and set  $\alpha = 1$ ,  $\mu = 0$ ,  $\Lambda = I$ ,  $a_1 = 10^4$ , and  $a_2 = b = 10$ . The true value of  $K$  is 4 and the true value of  $C$  is 10. For each dataset, we also generate a test set of 50 samples with 10,000 sequencing reads per sample. For the test set, we use  $\alpha = 1$  to generate the  $\phi_d$  and use the same  $\mu_k$  and  $\Sigma_k$  as the training set to generate the  $\psi_{d,k}$ .

First, fixing the modelled value of  $C$  to its true value (which we will later relax), we computed average perplexity results across the 200 datasets for LDA and LTN-LDA as we varied the number of modelled subcommunities  $K$  in Figure 4a. There are three main observations: (a) LTN-LDA significantly outperforms LDA for  $K$  near truth, (b) the perplexity curve for LTN-LDA decreases until it stabilizes at the true value of  $K$ , (c) the perplexity curve for LDA continues to decrease if the modelled  $K$  is increased past its true value.

We believe that the main reason that the two models behave so differently is that LDA

interprets the presence of cross-sample heterogeneity as extra subcommunities and so will find as many subcommunities as are modelled. This improves out of sample predictive performance but does not improve inference to truth. Thus, using perplexity to select the modelled number of subcommunities for LDA is a poor method if there is significant cross-sample heterogeneity. LTN-LDA is more robust and parsimonious in its representation of the data because it incorporates cross-sample heterogeneity in subcommunity compositions.

Fixing the modelled value of  $K$  to its true value, we computed average perplexity results across the 200 datasets for LTN-LDA as we varied the modelled  $C$  in Figure 4b. Note that LTN-LDA with  $C = 0$  is similar to LDA as it allows only very small levels of cross-sample heterogeneity and so may be taken as a point of comparison. The perplexity curve shows the same behavior as it did above: it decreases until it stabilizes at the true value of  $C$ .

Besides the perplexity, for the same datasets, we also computed the  $L_2$  distances between posterior mean estimates and true values for the  $\phi_d$ ,  $\beta_{d,k}$ , and  $\beta_k$  distributions (Figure 4c). The  $L_2$  distances allow us to assess how close posterior estimates are to truth. Unlike the perplexity curves, which stabilize after reaching the true value of  $C$ , the  $L_2$  distances are lowest around the true cutoff point  $C = 10$ . Thus, if the modelled value of  $C$  is increased too far above its true value, inference becomes reliable.

The above results suggest a simple two-stage strategy for choosing tuning parameters for LTN-LDA using perplexity. In the first stage, let  $K$  and  $C$  vary jointly on a grid and use either a test set or cross-validation to compute the average perplexity. This gives  $K$  perplexity curves over  $C$ . Set  $C$  to be the inflection point in these curves. In the second stage, vary  $K$  and set the value of  $K$  to be the inflection point of the resulting perplexity curve. Note that this strategy may fail for LDA. As our numerical examples show, due to

the lack of cross-sample heterogeneity in LDA the perplexity score generally continues to improve as one increase the number of subcommunities beyond its true value. This in turn leads to misleading inference on subcommunity abundance and subcommunity composition.

## 4 Evaluation on a microbiome study

We apply LTN-LDA to identify subcommunity dynamics in the dataset of [Dethlefsen and Relman \[2011\]](#), which has been previously investigated by other authors using LDA [[Sankaran and Holmes, 2019](#)]. The data includes the gut microbiome composition of three patients who were administered two five-day courses of ciprofloxacin over a ten-month span. For ease of comparison, we follow [Sankaran and Holmes \[2019\]](#) and focus on the 54 samples from patient F collected at uneven intervals and each of approximately 10,000 ASVs. The antibiotic regimens were given in two intervals: samples 12-23 and samples 41-51.

There are 2,852 unique ASVs in the dataset used in [Sankaran and Holmes \[2019\]](#). We merged ASVs into taxa at their finest known taxa and pruned all taxa which total at least 100 sequencing reads across all 54 samples. This left 44 taxa totalling 99.86 percent of the original counts. The resulting phylogenetic tree is included in the supporting information section S3.

We implemented the strategy outlined above to choose tuning parameters. In particular, we implement a 4-fold cross-validation letting  $K$  vary in  $\{2, 3, \dots, 8\}$  and  $C$  in  $\{1, 2, \dots, 21\}$ . The resulting  $K$  perplexity curves over  $C$  are presented in Figure [5a](#). The inflection point in the curve appears at  $C = 8$  and so we choose this value for  $C$ . Varying the modelled  $K$  gives the results in Figure [5b](#). For comparison, we applied LDA to the data over varying  $K$ . LTN-LDA has strictly lower perplexity than LDA across all modelled values of  $K$ , indicating

that there are significant levels of cross-sample heterogeneity in the dataset. Moreover, LTN-LDA experiences a noticeable inflection point (near 5) in contrast to LDA whose perplexity decays slowly over a much wider range of  $K$ .

We now present more detailed analysis for LTN-LDA and LDA with  $C = 8$ . For  $K \in \{3, 4, 7\}$  we plotted the subcommunity abundance on the left side of Figure 6. The grey regions indicate time periods when patient  $F$  underwent antibiotic treatment. As there were a small number of subcommunities, we manually corrected for label switching.

The subcommunities found by LTN-LDA are remarkably stable as  $K$  changes: subcommunities 1, 2, and 3 have almost the exact same abundance. Moreover, LTN-LDA finds that additional subcommunities have minimal abundance. LDA, however, finds as many subcommunities as are modelled: it splits heterogeneous subcommunities into subcommunities with no heterogeneity. For  $K = 7$ , we plotted the ASV-subcommunity distributions on the right side of Figure 6. Distributions for the  $\beta_{d,k}$  are in blue and the  $\beta_k$  are in red, while the LDA distributions are in black. The 5 most prevalent ASVs in each subcommunity are presented in Figure 7 for both LDA and LTN-LDA. LTN-LDA finds significant levels of cross-sample heterogeneity and provides meaningfully different subcommunity compositions than LDA.

We now analyze the three stable subcommunities found by LTN-LDA. The first subcommunity, composed mostly of Lachnospiraceae and Ruminococcaceae, falls off during periods of antibiotic treatment and recovers otherwise. The second subcommunity, composed mainly of Bacteroides, increases in abundance during the antibiotic treatments: this may indicate that it is more antibiotic-resistant than the first subcommunity. Both of these phenomena have been observed in mice [Zhu et al., 2020] and humans [Stewardson et al., 2015]. The third subcommunity is much less abundant, with a small spike only on the first day of the

second antibiotic course, but does persist as  $K$  changes. It is composed mostly of *Dialister* and *Veillonella*. Ciproflaxin has been shown to be effective against *Dialister* [Morio et al., 2007] which may explain the decrease in this subcommunity after treatment began.

## 5 Discussion

We have proposed a novel mixed-membership model which seeks to appropriately incorporate cross-sample heterogeneity in subcommunity compositions: a characteristic of the data prevalent in most microbiome studies. By incorporating the logistic-tree normal model for the sample-specific compositions of each subcommunity, we explicitly allow the composition of subcommunities to vary across samples. We have shown that incorporating cross-sample heterogeneity into MM models can lead to substantially improved inference. In particular, the popular strategy of overspecifying the number of subcommunities is only reasonable when such heterogeneity is accounted for. LTN-LDA is thus substantially more robust than LDA with respect to such overspecification. LTN-LDA also significantly outperforms LDA in terms of predictive performance as measured by perplexity in the presence of cross-sample heterogeneity. Moreover, in such contexts, predictive score can be a useful device to set the tuning parameters for LTN-LDA but not for LDA. Posterior computation on the LTN-LDA can proceed through collapsed blocked Gibbs-sampling with the assistance of Pólya-Gamma augmentation, and as such implementation for LTN-LDA is convenient.

We believe that the idea of incorporating cross-sample heterogeneity in MM models could be valuable beyond the context of microbiome compositions. In topic models, for example, one might expect different authors to write on the same topic using different vocabulary. LTN-LDA has the potential to be applicable to these other contexts as well, though the

immediate challenge which must be overcome is finding an appropriate tree structure.

## Acknowledgments

LM’s research is partly supported by NIGMS grant R01-GM135440 and NSF grant DMS-1749789. Part of the research was completed when PL was supported by an IBIEM fellowship at Duke University.

## References

- John Aitchison. The statistical analysis of compositional data. *Journal of the Royal Statistical Society. Series B (Methodological)*, 44(2):139–177, 1982.
- Francesco Beghini, Lauren J McIver, Aitor Blanco-Míguez, Leonard Dubois, Francesco Asnicar, Sagun Maharjan, Ana Mailyan, Paolo Manghi, Matthias Scholz, Andrew Maltez Thomas, Mireia Valles-Colomer, George Weingart, Yancong Zhang, Moreno Zolfo, Curtis Huttenhower, Eric A Franzosa, and Nicola Segata. Integrating taxonomic, functional, and strain-level profiling of diverse microbial communities with biobakery 3. *Elife*, 2021.
- David M. Blei, Andrew Y. Ng, and Michael I. Jordan. Latent dirichlet allocation. *Journal of Machine Learning Research*, 3:993–1022, 2003.
- Benjamin J Callahan, Paul J McMurdie, and Susan P Holmes. Exact sequence variants should replace operational taxonomic units in marker-gene data analysis. *The ISME Journal*, 11:2639–2643, 2017.
- Paul I. Costea, Falk Hildebrand, Manimozhiyan Arumugam, Fredrik Backhed, Martin J. Blaser, Frederic D. Bushman, Willem M. de Vos, S. Dusko Ehrlich, Claire M. Fraser,

- Masahira Hattori, Curtis Huttenhower, Ian B. Jeffery, Dan Knights, James D. Lewis, Ruth E. Ley, Howard Ochman, Paul W. O’Toole, Christopher Quince, David A. Relman, Fergus Shanahan, Shinichi Sunagawa, Jun Wang, George M. Weinstock, Gary D. Wu, Georg Zeller, Liping Zhao, Jeroen Raes, Rob Knight, and Peer Bork. Enterotypes in the landscape of gut microbial community composition. *Nature Microbiology*, 3:8–16, 2018.
- Rebecca A Deek and Hongzhe Li. A zero-inflated latent dirichlet allocation model for microbiome studies. *Frontiers in Genetics*, 11:599–614, 2019.
- Federica Del Chierico, Pamela Vernocchi, Bruno Dallapiccola, and Lorenza Putignani. Mediterranean diet and health: Food effects on gut microbiota and disease control. *International Journal of Molecular Sciences*, 15(7):11678–11699, 2014.
- Les Dethlefsen and David A. Relman. Incomplete recovery and individualized responses of the human distal gut microbiota to repeated antibiotic perturbation. *Proceedings of the National Academy of the Sciences of the United States of America*, 108(Supplement 1):4554–4561, 2011.
- Chris Glynn, Surya T. Tokdar, Brian Howard, and David L. Banks. Bayesian Analysis of Dynamic Linear Topic Models. *Bayesian Analysis*, 14(1):53 – 80, 2019.
- Thomas L. Griffiths and Mark Steyvers. Finding scientific topics. *Proceedings of the National Academy of Sciences*, 101(suppl 1):5228–5235, 2004.
- Ian Holmes, Keith Harris, and Christopher Quince. Dirichlet multinomial mixtures: Generative models for microbial metagenomics. *PLoS ONE*, 7(2), 2012.

- Hongzhe Li. Microbiome, metagenomics, and high-dimensional compositional data analysis. *Annual Review of Statistics and Its Application*, 2(1):73–94, 2015.
- Jialiang Mao, Yuhao Chen, and Li Ma. Bayesian graphical compositional regression for microbiome data. *Journal of the American Statistical Association*, 115(530):610–624, 2020.
- F. Morio, H. Jean-Pierre, L. Dubreuil, E. Jumas-Bilak, L. Calvet, G. Mercier, R. Devine, and H. Marchandin. Antimicrobial susceptibilities and clinical sources of dialister species. *Antimicrobial Agents and Chemotherapy*, 51(12):4498–4501, 2007.
- Kamal Nigam, Andrew Kachites McCallum, Sebastian Thrun, and Tom Mitchell. Text classification from labeled and unlabeled documents using em. *Machine Learning*, 39:103–134, 2000.
- Nicholas G. Polson, James G. Scott, and Jesse Windle. Bayesian inference for logistic models using pólya–gamma latent variables. *Journal of the American Statistical Association*, 108(504):1339–1349, 2013.
- Kris Sankaran and Susan P Holmes. Latent variable modeling for the microbiome. *Biostatistics*, 20(4):599–614, 2019.
- Mahdi Shafiei, Katherine A Dunn, Eva Boon, Shelley M MacDonald, David A Walsh, Hong Gu, and Joseph P Bielawski. Biomico: a supervised bayesian model for inference of microbial community structure. *Microbiome*, 3(8), 2015.
- A.J. Stewardson, N. Gaia, P. Francois, S. Malhotra-Kumar, C. Delemont, B. Martinez de Tejada, J. Schrenzel, S. Harbarth, and V. Lazarevic. Collateral damage from oral



- ciprofloxacin versus nitrofurantoin in outpatients with urinary tract infections: a culture-free analysis of gut microbiota. *Clinical Microbiology and Infection*, 21(4):344.e1–344.e11, 2015.
- Yunfan Tang, Li Ma, and Dan L. Nicolae. A phylogenetic scan test on a Dirichlet-tree multinomial model for microbiome data. *The Annals of Applied Statistics*, 12(1):1–26, 2018.
- Hanna M. Wallach, Iain Murray, Ruslan Salakhutdinov, and David Mimno. Evaluation methods for topic models. *Proceedings of the 26th Annual International Conference on Machine Learning*, page 1105–1112, 2009.
- Tao Wang and Hongyu Zhao. A dirichlet-tree multinomial regression model for associating dietary nutrients with gut microorganisms. *Biometrics*, 73(3):792–801, 2017.
- Zhuoqun Wang, Jialiang Mao, and Li Ma. Microbiome compositional analysis with logistic-tree normal models. <https://arxiv.org/abs/2106.15051>, 2021.
- Shengyun Zhu, Huiqi Li, Jing Liang, Chaoran Lv, Kai Zhao, Mingshan Niu, Zhenyu Li, Lingyu Zeng, and Kailin Xu. Assessment of oral ciprofloxacin impaired gut barrier integrity on gut bacteria in mice. *International Immunopharmacology*, 83, 2020.

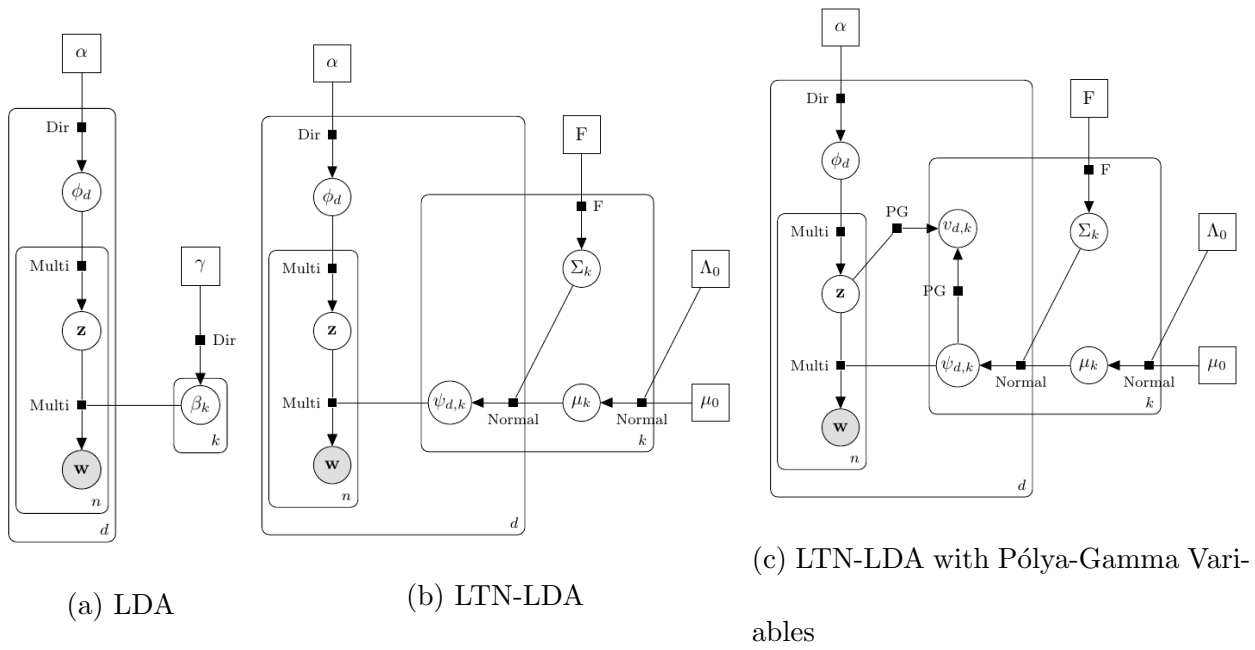


Figure 1: Graphical model representations for LDA and LTN-LDA.

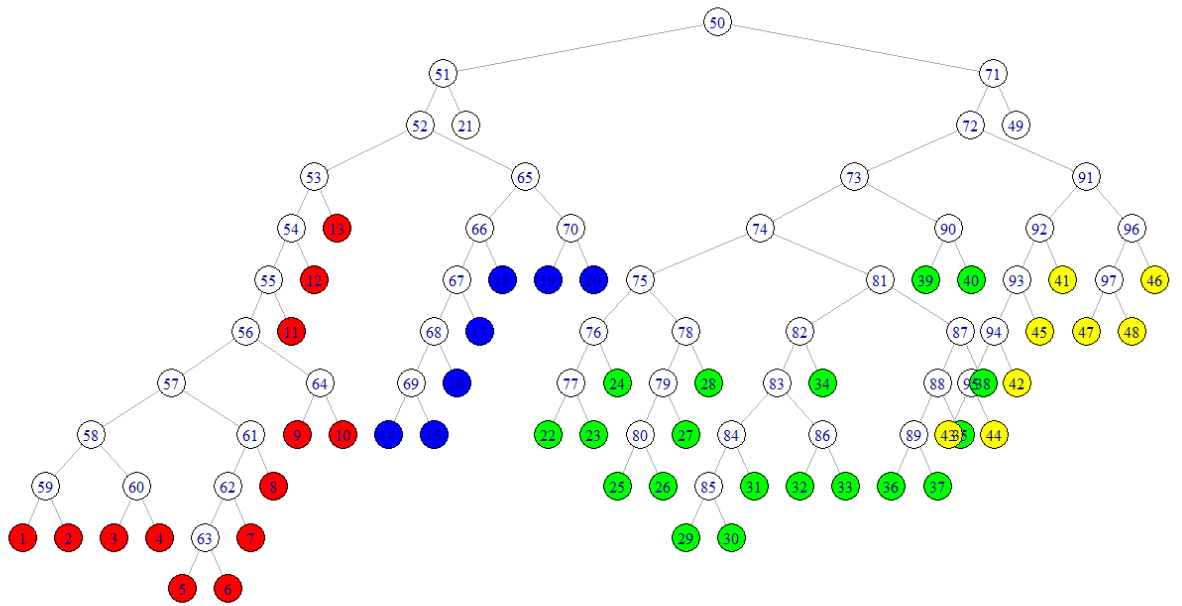


Figure 2: The phylogenetic tree used in simulations

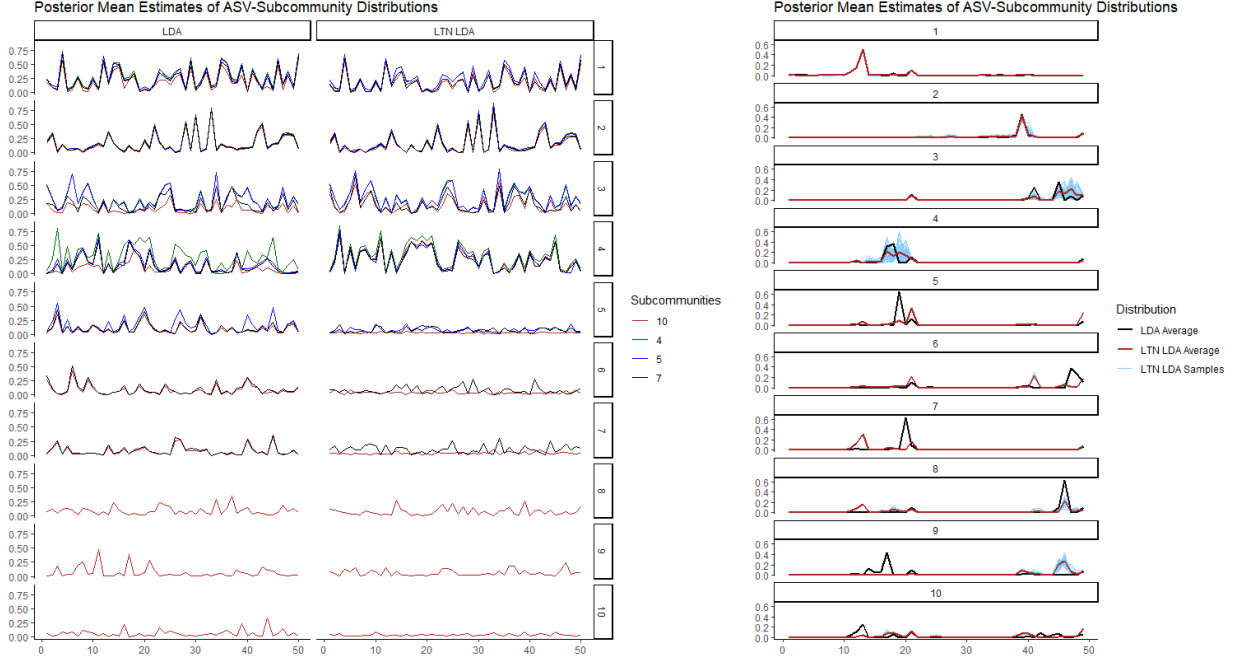


Figure 3: (Left) Subcommunity abundance for  $\phi_d$  for all samples over four different numbers of subcommunities  $K \in \{4, 5, 7, 10\}$  for LDA (left) and LTN-LDA (right). The estimated abundances are noticeably more stable over different values of  $K$  for the LTN-LDA. (Right) Estimated subcommunity compositions for all samples. Blue indicates the sample-specific composition under LTN-LDA ( $\beta_{d,k}$ , red indicates the average subcommunity composition under LTN-LDA ( $\beta_k$ ) and black indicates the average subcommunity composition ( $\beta_k$ ) under LDA. The 49 ASVs are on the x-axis.

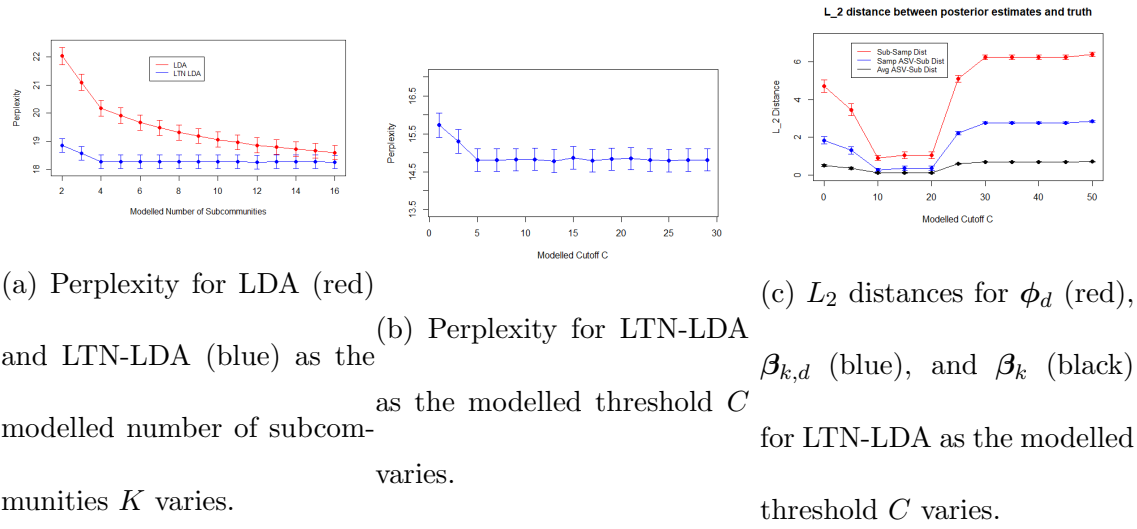
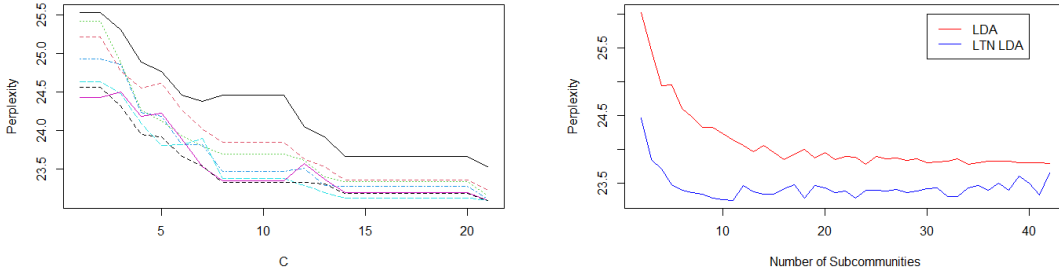


Figure 4: Simulation Results



(a) Perplexity for varying levels on  $K$  on the (b) Perplexity for LTN-LDA and LDA as  $K$   
Dethlefsen and Relman data as we vary  $C$  varies while  $C = 8$ .

Figure 5: Cross-validation results

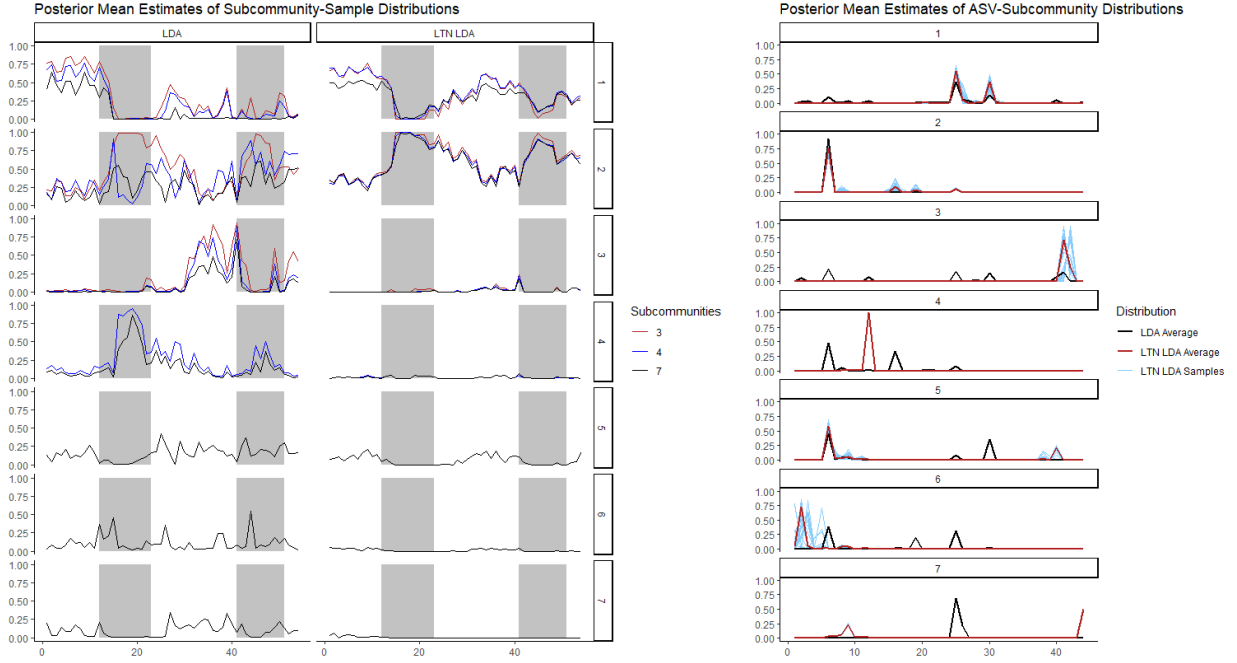


Figure 6: (Left) Subcommunity abundance for  $\phi_d$  for all samples over three different numbers of subcommunities  $K \in \{3, 4, 7\}$  for LDA (left) and LTN-LDA (right). The estimated abundances are noticeably more stable over different values of  $K$  for the LTN-LDA. (Right) Estimated subcommunity compositions for all samples. Blue indicates the sample-specific composition under LTN-LDA ( $\beta_{k,d}$ , red indicates the average subcommunity composition under LTN-LDA ( $\beta_k$ ) and black indicates the average subcommunity composition ( $\beta_k$ ) under LDA. The 44 ASVs are on the x-axis.

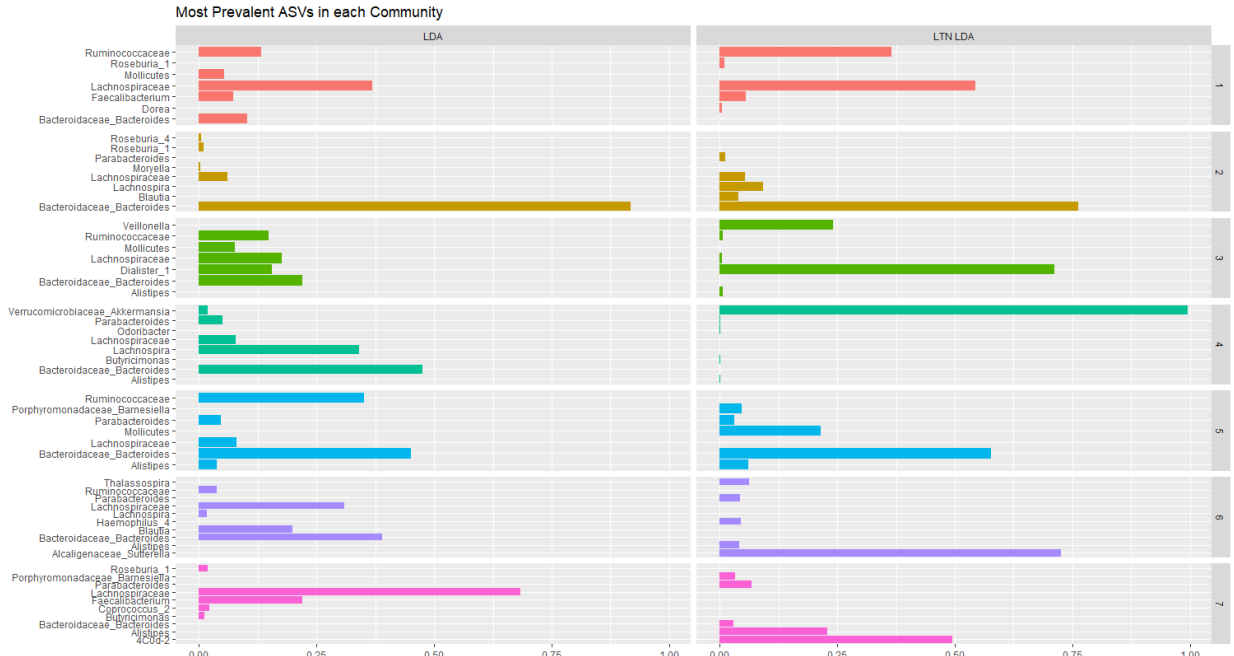


Figure 7: The 5 most prevalent ASVs in each subcommunity for LDA and LTN-LDA,  $K = 7$ ,

$C = 8$ .



## Software

The version of the dataset used in Sankaran and Holmes [2019] is available at [https://github.com/krisrs1128/microbiome\\_plvm/tree/master/data/antibiotics-study](https://github.com/krisrs1128/microbiome_plvm/tree/master/data/antibiotics-study). Reproducible code and data for this paper is available <https://github.com/PatrickLeBlanc/ReproduceLTNLDAPaper>. R code for implementing the LTN-LDA model is available in the LTNLDA package <https://github.com/PatrickLeBlanc/LTNLDA>.

## 6 Supporting Information

### 6.1 S1

Figure 8 is an example phylogenetic tree. In this case,  $\mathcal{L} = \{1, 2, 3, 4, 5, 6\}$ ,  $\mathcal{I} = \{7, 8, 9, 10, 11\}$ . The root node 7 can be represented with the set  $\{1, 2, 3, 4, 5, 6\}$  while node 8 can be represented with the set  $\{1, 2\}$ . If node 7 is  $A$ , then  $A_l$  is 8 and  $A_r$  is 9.

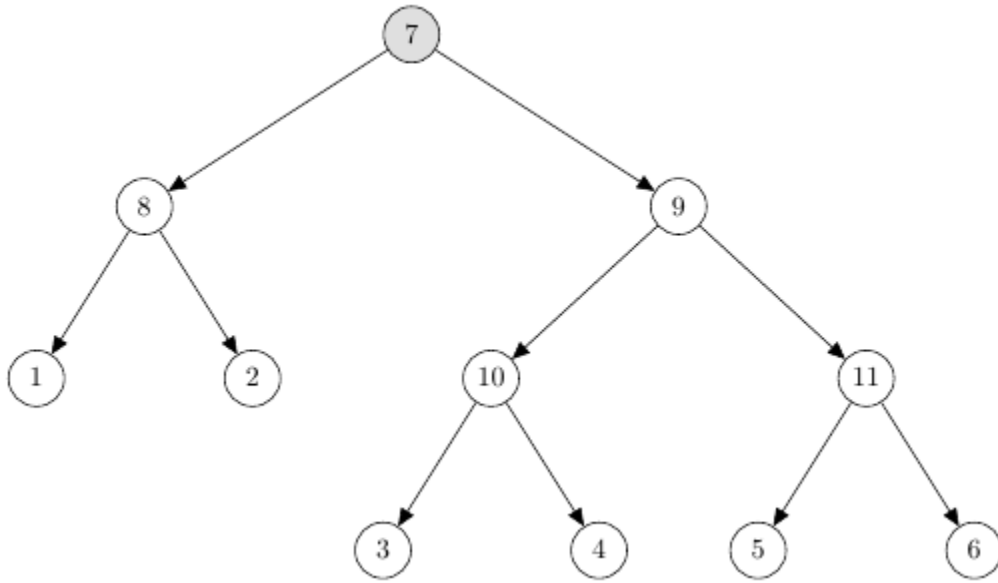


Figure 8: An example phylogenetic tree

## 6.2 S2

Perplexity is a transformation of predictive log-likelihood commonly used to assess topic models. If  $p(\mathbf{w}_{d^{(te)}}|\mathcal{M})$  is the predictive log-likelihood of a test set sample  $d^{(te)}$  given a collection of parameters  $\mathcal{M}$ , then perplexity is defined as

$$\exp\left(-\frac{\sum_d p(\mathbf{w}_{d^{(te)}}|\mathcal{M})}{\sum_d N_{d^{(te)}}}\right),$$

where  $N_{d^{(te)}}$  is the number of sequencing reads in  $d^{(te)}$

The document completion method for computing perplexity for LDA is described in section 5 of [Wallach et al. \[2009\]](#). It involves splitting each sample  $d^{(te)}$  in the test set into two halves,  $d^{(te),1}$  and  $d^{(te),2}$ . A modified Gibbs sampler is run on the first half,  $d^{(te),1}$  with the value of  $\beta_k$  set equal to the posterior mean of  $\beta_k$  on the training set. The results of this Gibbs sampler are used to develop estimates for  $\phi_d$  and then for perplexity.

We modify this procedure for LTN-LDA. A modified Gibbs is run on  $d^{(te),1}$ , fixing the values of  $\mu_k$  and  $\Sigma_k$  at their posterior means from the training set. If there are  $I$  iterations in the Gibbs sampler, then the estimate of  $\phi_d$  at iterate  $i$  is  $\phi_d(i)$  and the estimate of  $\beta_{d,k}$  of iterate  $i$  is  $\beta_{d,k}(i)$ . We can then take a Monte Carlo estimate over all ASVs observed in  $d^{(te),2}$  to estimate the predictive likelihood of  $d^{te}$ :

$$\frac{1}{I} \sum_{i=1}^I \sum_{n \in \mathbf{w}_{d^{(te)},2}} \log \left( \sum_{k=1}^K \phi_d^k(i) \beta_{d,k}^{w_{d,n}}(i) \right).$$

This procedure can be repeated for every sample in the test set, and the resulting set of predictive likelihood estimates can be transformed into a perplexity estimate.

### 6.3 S3

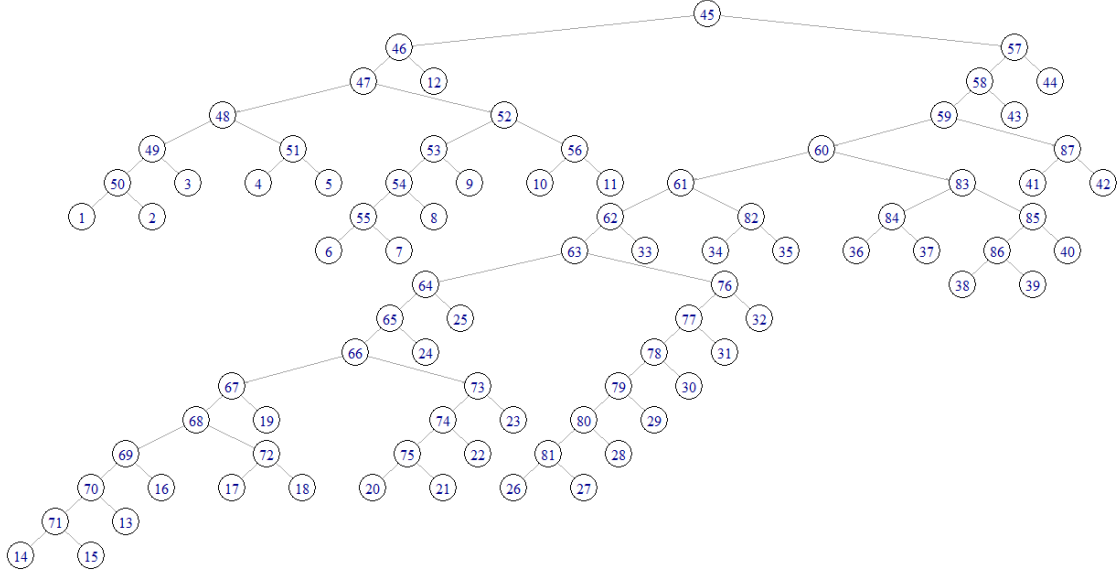


Figure 9: The tree resulting from the dataset of [Dethlefsen and Relman \[2011\]](#)